ORIGINAL ARTICLE

Assessment of defoliation and subsequent growth losses caused by *Lymantria dispar* using terrestrial laser scanning (TLS)

Martin Jacobs[1] · Torben Hilmers[1] · Benjamin M. L. Leroy[2] · Hannes Lemme[6] · Sebastian Kienlein[2,3] · Jörg Müller[4,5] · Wolfgang W. Weisser[2] · Hans Pretzsch[1]

Abstract

Key message TLS scans of three surveys before, during and after gypsy moth gradation, allowed high-resolution tracking of defoliation and subsequent inter-annual growth losses on an individual tree level.

Abstract Foliation strongly determines all tree growth processes but can be reduced by various stress factors. Insect defoliation starts at variable times and is one stress factor that may affect photosynthetic processes and cause immediate reactions like refoliation, which are difficult to detect by surveys repeated at 1-year intervals. This study used a large-scale field experiment in German oak/mixed forests affected by gypsy moths (*Lymantria dispar*) to test the use of terrestrial laser scanning (TLS) for detecting inter-annual foliation and growth losses at the individual tree level caused by the gypsy moth. The experiment comprised two levels of gypsy moth defoliation risk, high (H) and low (L), as well as two pest control treatment levels: spraying with the insecticide Mimic (M) or unsprayed control (C). The factorial design consisted of four treatment combinations (HC, HM, LC, and LM), applied to 11 spatial blocks with a total of 44 plots. The TLS approach detected the defoliation caused by the gypsy moth, estimated as leaf area and crown perforation parameters. For the first time, TLS-derived tree foliation was evaluated based on inter-annual stem growth. Leaf area and crown perforation showed a correlation of + 0.6 and – 0.35, respectively, with basal area increments. Furthermore, this study revealed subsequent growth losses in the same year due to defoliation. Our results show that TLS can offer new opportunities to develop new indicators that monitor foliation at the individual tree level. The crown perforation can describe defoliation or the tree's vitality based on one scanning campaign, whereas the leaf area needed at least two.

Keywords Oak · Crown transparency · Leaf area · Infestation · Crown projection area · Monitoring

✉ Martin Jacobs
martin.jacobs@tum.de

1 Chair of Forest Growth and Yield Science, Department of Life Science Systems, TUM School of Life Sciences, Technical University of Munich, Hans-Carl-von-Carlowitz-Platz 2, 85354 Freising, Germany

2 Terrestrial Ecology Research Group, Department of Life Science Systems, TUM School of Life Sciences, Technical University of Munich, Freising, Germany

3 Ecosystem Dynamics and Forest Management Research Group, Department of Life Science Systems, TUM School of Life Sciences, Technical University of Munich, Freising, Germany

4 Field Station Fabrikschleichach, Department of Animal Ecology and Tropical Biology, Biocenter, University of Würzburg, Rauhenebrach, Germany

5 Bavarian Forest National Park, Grafenau, Germany

6 Department of Forest Protection, Bavarian State Institute of Forestry, Freising, Germany

Introduction

The frequency and intensity of insect-induced forest disturbances is set to rise due to climate change and changes in forest structure and composition (Seidl et al. 2011). Consequently, effective methods that can detect and quantify stress factors are needed. One important stress factor is insect defoliation, which causes a significant reduction in tree growth (Piper et al. 2015). Whereas stem growth is easy to measure, the exact calculation of a tree's foliation is difficult. There is no suitable reference for evaluation. Traditional defoliation assessments, e.g., by eye or using fisheye photographs, have been criticised as being highly subjective (Dobbertin 2005), while current foliation determination approaches based on spectral information from TLS return intensity or machine learning are complex and expensive (Calders et al. 2020). As a result, a simple and reliable procedure is required, the results of which were compared to a suitable reference. In contrast to the approaches available, we evaluated our calculated foliation parameters based on inter-annual stem growth since stem growth and leaf area are correlated (Rolland et al. 2001).

With regard to defoliation, the gypsy moth (*Lymantria dispar*) is one of the most critical pest species of hardwood forests in its introduced range in North America and its native range in temperate Europe, North Africa, and Asia (Montgomery and Wallner 1988). Introduced roughly 150 years ago into the eastern part of the United States, the species spread across most of East Canada (Liebhold et al. 1992), causing overall annual damage of $3.4 billion in North America (Bradshaw et al. 2016). In its native range, it can cause severe damage during outbreaks, e.g., in Europe, but it is mostly known for its severe impacts and rapid expansion in North American forests, where it is invasive (McManus and Csóka 2007). Severe defoliation, range expansion, and increasing gypsy moth frequencies, exacerbated by rising temperatures (Logan et al. 2003), have also been reported in Central Europe (McManus and Csóka 2007), Russian Far East and Central Asia (Gninenko and Orlinskii 2003; Orozumbekov et al. 2009) and North Africa (Villemant and Ramzi 1995). However, it is not an invasive species in Europe and Asia yet.

Defoliation can have effects on forest structure and stand development. In addition, defoliation and tree mortality may also affect the community composition of tree regeneration and herbaceous vegetation through interspecies competition effects in the sub-canopies, triggered by the increased light availability in the canopy gaps (Fajvan and Wood 1996). Furthermore, Nakajima (2015) suggested that insect defoliation can dramatically affect forest ecosystem processes, such as the regeneration of host trees and the behavior of wildlife that depend on

seed production, by reducing the reproductive potential of host trees. At single-tree level, defoliation affects the condition, causing significantly reduced timber production (Piper et al. 2015). In detail, tree defoliation can result in growth loss (Naidoo and Lechowicz 2001), reduced root biomass production (Thomas et al. 2002), and increased tree mortality compared to non-outbreak situations (Elling et al. 2007). Here, tree mortality depends on the frequency, intensity, duration, and combination of defoliation, the vitality status of the infested trees, and biotic or abiotic stresses (Elling et al. 2007). Severe insect defoliation as a stress factor directly affects the photosynthetic processes and indirectly reduces stem growth (Dobbertin 2005). Defoliation also induces the formation of a light ring consisting of thin-walled latewood tracheids in larch trees, which would affect timber quality (Watanabe and Ohno 2020). This is also proven for oak trees and may also affect tree vitality (Blank 1997). The study by Gieger and Thomas (2002) revealed for both *Quercus robur* L. and *Quercus petraea* (Matt.) Liebl. that defoliation—solely or in combination with drought—and subsequent growth loss result in a deteriorated water supply after embolism, reducing the tree's vitality. When several damaging factors coincide, such as defoliation and late frost or defoliation and drought, this may lead to the death of the oaks (Gieger and Thomas 2002). According to Fajvan et al. (2008), the defoliation of oaks by gypsy moth reduced volume growth increment and wood strength properties more in the upper stem sections than in the lower bole. In summary, defoliation by insects is a critical stress factor affecting the photosynthetic processes, carbon allocation, and thus tree growth (Dobbertin 2005). Tree growth is the increase in size and in the tree's number of vegetative structures, consisting of leaves, stem and roots, while leaf growth is the most critical tree growth process (Waring 1987).

Analysing the relationship between insect defoliation and tree growth is not simple. Insect defoliation has been shown to influence tree growth and can be reconstructed from tree rings (Rolland et al. 2001). For example, periodically reoccurring outbreaks of the larch bud moth (*Zeiraphera diniana* Gn) in the European Alps were shown to lead to reduced ring widths in the European larch (*Larix decidua* Mill) (Rolland et al. 2001). Additionally, the leaf area has been found to correlate well with the sapwood area at breast height (Waring et al. 1981) or with the sapwood area without the latewood (Eckmüllner and Sterba 2000). As the effect of the outbreaks is usually compensated for during non-outbreak periods, the effects of insect defoliation on tree growth cannot be detected in forest inventories carried out in one or 5-year growth intervals (Dobbertin 2005). For that reason, inter-annual stem growth and leaf area should be assessed together (Dobbertin 2005).

Whereas measuring stem growth is simple, determining leaf area is more difficult due to accessibility issues. Because the destructive assessment of a tree's original leaf area size is rarely feasible, the visual assessment of tree crowns and their classification into transparency or defoliation classes is a standard procedure in many parts of the world and can be carried out cost-effectively and relatively quickly in field surveys (Müller-Edzards et al. 1997). However, crown transparency assessments are under criticism due to their high level of subjectivity (Dobbertin et al. 2009). Furthermore, they require intensive training courses and repeated control assessments (Wulff 2002). For crown transparency assessments, no absolute reference is known. Instead, only site-specific reference trees are used (Innes 1993). Satellite-based approaches for forest canopy condition monitoring may provide insights into broad-scale forest health dynamics with a relatively fine spatial and temporal resolution (Pasquarella et al. 2018) but not at individual tree level. Collection of the leaves with leaf trap baskets is laborious and not applicable over a large area. Leaves can also be carried away by wind. Consequently, there is a need for new rational measurement methods with a fast and easily understandable procedure for determining a single tree's foliation. In addition, a method is required that is able to take objective measurements several times a year to record the temporal change in the crown condition. Starting with the beginning of the leaf growth, the temporally variable onset of insect feeding, which, depending on the intensity, also leads to leaf regrowth, a very high dynamic is formed in the vegetation period.

TLS has been used to address numerous information gaps in traditional inventory data (Calders et al. 2020). Ground-based LiDAR measurements can thereby be an alternative to airborne LiDAR observations, depending on the information needed, especially at the single-tree level (Hilker et al. 2010). In particular, it is possible to determine the structural crown properties of trees independently of tree species (Bayer et al. 2013). TLS has the potential and ability to scan and reach the canopy area successfully (Seidel et al. 2015). Several studies have already shown how to detect single tree defoliation at tree and stand level via TLS (Huo et al. 2019; Kaasalainen et al. 2010). The methodology of leaf area determination and classification into wood and leaf material is challenging. Leaf-wood separation approaches based on spectral information from TLS return intensity or machine learning are complex and expensive (Calders et al. 2020), making them difficult to reproduce. Therefore, robust and simple methods are required.

This study shows some simple new methods for the efficient monitoring of foliation at an individual tree level via terrestrial laser scanning (TLS), using the example of oak/mixed forests in Germany. Here, we used a novel approach to assess tree defoliation and link it to tree growth. In contrast to the TLS leaf-wood separation approaches available,

we evaluated our calculated foliation parameters based on inter-annual stem growth since stem growth and leaf area are correlated (Rolland et al. 2001). To show the effects of defoliation, we used a large-scale field experiment in gypsy moth-infested oak-mixed forests in Germany (Leroy et al. 2021). The experimental design comprises two defoliation risk levels based on gypsy moth egg-mass occurrence and two treatment types sprayed to protect the trees from defoliation or unsprayed control. Based on TLS and the large-scale field experiment, the current study focused on the scan and quantification of the leaf area status using the TLS point clouds of three subsequent surveys before and after the gypsy moth infestation. We also focused on the development of the parameter crown perforation, which describes the foliation based on only one TLS survey in the growing season.

The study addressed the following research questions:

Q1: Does the leaf area and crown perforation calculated using TLS differ between trees attacked by gypsy moths and trees without damage?

Q2: Are leaf area and crown perforation related to stem increment within the same year?

Q3: Is the relationship between leaf area/crown perforation and basal area increment modified by the gypsy moth?

Material and methods

Experimental design

The experiment took place in mixed oak forests in different stands in Franconia-Bavaria in Germany (Leroy et al. 2021). The experimental design area consisted of 11 blocks (A, B, D, F, G, H, J, M, N, O, and S), varying spatially and dominated by oak trees. Each block was subdivided into four plots with similar forest structures, stand ages, and tree species composition within the block. Each plot had a mean size of 0.05 km^2 ($\pm$ SD 0.20). Within each block, two of the four plots had a high (H) defoliation risk, while the other two had a low (L) defoliation risk. For this classification, a defoliation risk index was used, which calculation was based primarily on gypsy moth egg-mass density (Leroy et al. 2021, Appendix). The survey of egg-mass density was conducted by regional forest offices in 2018 (Leroy et al. 2021). In each block, an insecticide treatment (Mimic; M) was randomly assigned to one plot per defoliation risk level, while the second plot was left unsprayed and used as a control (C). The treatment plots were sprayed with the insecticide tebufenozide as Mimic® (Spiess-Urania Chemicals, Hamburg, Germany; 240 g l^{-1} active ingredient) between May 3rd and May 23rd (124–144 days of the year, DOY) 2019 at the maximal legal rate of 750 ml ha^{-1}. The treatments were applied by helicopter under conditions

of dry and less-than-windy weather. In total, 44 plots were sampled, which had been selected to represent 11 weak and strong infestations, and 11 remained with and without control.

At each plot, 20 six-tree samples, including one central oak tree and the following five neighboring trees with a diameter at breast height ($d_{1.3}$) greater than or equal to seven cm, were sampled, so that 880 central trees and 4400 neighboring trees were used to describe the stand characteristics such as basal area, standing volume, etc. for each block (Table 1). Single tree volume was calculated based on basal area, total tree height and species specific form factors for all six-tree sample trees. The single tree volumes were summed up to standing volume for block level. For stand characteristics, the total tree heights and basal area were retrieved from TLS. To estimate the variables per ha, we calculated the expansion factor. For this, we measured the distance between the central oak tree and the fifth neighboring tree via TLS for all 80 six-tree samples per block. After that, we calculated the circular area for each six-tree sample using the measured distances as the radius. We summed up all the areas of one block, and then we divided 10,000 by this area to get the expansion factor to calculate the variables per ha. A more detailed description of the stand characteristics per plot can be found in Table 4 in the Appendix. The 20 six-tree samples were established along transects in the four main cardinal directions (Fig. 1), starting from the centre of each sampling plot. Six-tree samples were taken at 25, 50, 75, 100, and 125 m from the centre of each plot (origin of the coordinate system in Fig. 1). More detailed information on the experiment and its design can be found in (Leroy et al. 2021).
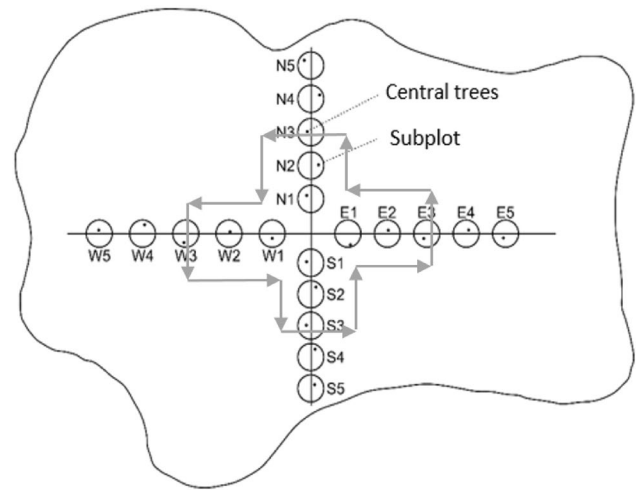

Fig. 1 An overview of a plot with 20 six-tree subplots along transects in the main cardinal directions, starting from the centre of the infested area For the detailed analysis, each six-tree subplot yields one central tree and five neighboring trees with $d_{1.3}$ greater than or equal to seven cm. The surveys were carried out along the transect using TLS in the winter. The grey arrows signify the scanning direction of TLS campaigns two and three in summer in relation to leaf area detection

Methods

The 880 central oak trees of each six-tree sampling were equipped with long-term girth tapes to analyse the inter-annual stem growth during the 2019 growing season. We measured the tree positions (x- and y-coordinates), the distances between the trees and the total tree heights via TLS. The following demonstrates the different steps of the TLS method applied. A detailed description of the workflow of the TLS procedure can be found in the Appendix: 1. Scanner

Table 1 The stand characteristics of the 11 blocks in Franconia-Bavaria, Germany

Block	n (ha^{-1})	dq (cm)	hq (m)	BA (m^2 ha^{-1})	SV (m^3 ha^{-1})
A	**493** (339–713)	**23.0** (7.1–71.5)	**17.6** (5.2–26.6)	**26.8** (23.5–30.1)	**235.3** (218.3–265.0)
B	**424** (314–622)	**25.5** (7.6–61.6)	**19.8** (6.3–27.4)	**26.0** (22.5–30.5)	**256.8** (211.1–313.5)
D	**563** (357–753)	**23.0** (7.0–76.0)	**17.4** (6.1–29.2)	**34.0** (27.7–40.1)	**296.6** (258.0–364.6)
F	**260** (200–467)	**33.3** (7.6–85.7)	**22.9** (6.0–33.1)	**28.0** (22.7–36.4)	**319.2** (240.3–373.3)
G	**415** (261–632)	**24.7** (7.0–69.8)	**17.8** (3.1–30.6)	**28.6** (27.7–30.1)	**254.3** (230.5–301.0)
H	**517** (437–640)	**26.3** (7.0–66.9)	**20.6** (6.2–30.1)	**32.1** (29.0–34.3)	**329.7** (300.7–369.5)
J	**434** (294–718)	**26.2** (7.3–97.6)	**20.8** (4.5–34.4)	**30.5** (25.8–35.2)	**316.9** (281.3–356.5)
M	**411** (323–512)	**28.8** (7.3–78.2)	**20.9** (4.1–31.1)	**35.2** (28.7–41.7)	**367.9** (317.8–443.0)
N	**377** (293–474)	**26.2** (7.2–78.2)	**18.5** (4.4–28.1)	**26.8** (24.9–30.1)	**247.8** (228.1–272.5)
O	**287** (190–672)	**29.4** (8.0–83.7)	**20.3** (5.9–31.1)	**24.8** (20.5–36.1)	**252.1** (230.4–309.2)
S	**307** (305–350)	**29.9** (7.1–78.8)	**22.2** (5.0–33.0)	**29.0** (26.3–32.6)	**321.9** (305.4–349.7)

The parameters were calculated based on TLS point clouds using 5280 trees (six-tree subplots). Data from TLS survey in 2019, **mean** (range)

n number of trees, *dq* quadratic mean diameter, *hq* height corresponding to dq, *BA* basal area, *SV* standing volume

configuration and settings; 2. Data post-processing; 3. Tree detection and isolation; 4. Tree parameter extraction.

Terrestrial laser scanning acquisition

The terrestrial laser scanning (TLS) campaign was conducted to record the six-tree samplings in a leaf-off situation in winter to describe the forest stand characteristics (Table 1) and to determine the different status of forest canopy structures in three dimensions before and after insect defoliation. The RIEGL VZ-400i (RIEGL 2019) was used as a laser measurement system. A detailed description of the scanner configuration and settings can be found in the appendix.

The first scanning campaign (TLS_1) was carried out in early 2019, before the growing season in leaf-off conditions (79–107 DOY; 20th March–17th April, t_1). The second campaign (TLS_2) was conducted during the peak feeding of the gypsy moth between 179 and 200 DOY (28th June–19th July, t_2), and the third campaign (TLS_3) after the end of defoliation between 240 and 249 DOY (27th August–5th September, t_3). TLS_1 covered the total area of the subplots of each plot to describe the stand characteristics (Fig. 1, Table 1). As shown in Fig. 1 and marked by the grey arrows, TLS_2 and TLS_3 covered the area from the plot centre to the second subplot of each transect direction. Since all the plots needed to be scanned roughly simultaneously during the defoliation period, a smaller scan area was chosen for faster acquisition during the second and third campaigns. Consequently, the leaf area status was determined for eight trees per plot, resulting in 352 (44×8) trees in total. Their characteristics are described in Table 2. For all scanning campaigns, multiple scans were taken consecutively around the plots. The number of scan positions varied between the plots depending on the stand density of the plots. The higher the stand density, the more scan positions were needed. The number of scan positions per plot between the scanning campaigns t_2 and t_3 was always the same to ensure the comparability of the measurements (*ceteris paribus* conditions).

TLS data post-processing

The automatic registration of the LMS VZ-400i was applied so that artificial reference targets were not needed in the field. The automatic registration, filtering, and multi-station adjustment (MSA), which were used to refine the overall registration, were performed using the RiSCAN PRO version 2.10.1 software (http://www.riegl.com/products/software-packages/riscan-pro/). Using the automatic registration feature and since we started each scan at approximately the same position where we finished the previous scanning campaign at the specific plot, it was possible to register all the point clouds of each scanning campaign (TLS_1 to TLS_3) into one project coordinate system. To include all the foliage, stems, and branches (sometimes hidden by foliage) on t_2 and t_3, we merged each point cloud from TLS_2 and TLS_3 with the point clouds from TLS_1, before using an octree. This means that structural tree modifications within the scanning campaigns t_1 to t_3 can be directly visualised (Fig. 2). Every point cloud was reduced using an octree to enable fast point-cloud processing without accuracy loss (Elseberg et al. 2013). An octree is a tree data structure that is used for indexing three-dimensional data where one node has up to eight children, each responding to one octant of the overlying node. Therefore, the octree data structure is ideally suited to storing and retrieving three-dimensional laser scanner data efficiently (Elseberg et al. 2013). This way, the data are evenly distributed in space, whereby each cube with an edge length of five cm contains only one measuring point on average, set according to the centre of gravity of the cube's original points.

The complete processing was carried out within the programming environment of R (R Core Team 2016). For this purpose, the rlas package (Roussel and Boissieu 2019) was applied to import the .las files into R. Each central tree was marked with a reflector in the field during scanning. This made it possible to detect the central trees in all point clouds due to their higher reflectance values (> 1) compared to the rest of the points. After tree detection, the isolation of each central tree from the TLS point cloud of t_1, t_2, and t_3 was performed using a specifically developed preprocessing algorithm, which is based on the density-based spatial clustering

Table 2 Central oak tree characteristics of the four defoliation risk/treatment groups in Franconia-Bavaria, Germany, were calculated via TLS data where diameter at breast height ($d_{1.3}$) was recorded manually with long-term girth tape

Trees scanned for leaf area determination/mean[a] ($\pm$ SE)					
Group		High control	High mimic	Low control	Low mimic
Trees per group n		88	88	88	88
Diameter at breast height $d_{1.3}$	cm	42.7 (1.4)	42.8 (1.4)	43.4 (1.0)	45.4 (1.4)
Height h	m	23.5 (0.4)	24.1 (0.4)	25.0 (0.4)	24.7 (0.3)
Crown projection area *cpa*	m^2	45.9 (2.6)	51.0 (4.1)	49.0 (2.9)	54.2 (3.3)

[a]Data from the survey in 2019

Fig. 2 A bird's-eye view of two sample trees extracted from the TLS point cloud **a**, **c** in winter without leaves; **b**, **d** in summer during peak feeding. Tree no. 1 is a tree from a plot with a high defoliation risk and no treatment (HC, i.e., control); Tree no. 2 is a tree from an area with a high defoliation risk and treated with Mimic (HM). Tree no. 1 has a calculated leaf area of 5.9 m² and tree no. 2 has a leaf area of 38.3 m²

Tree no. 1

a

Tree no. 1

b

Tree no. 2

c

Tree no. 2

d
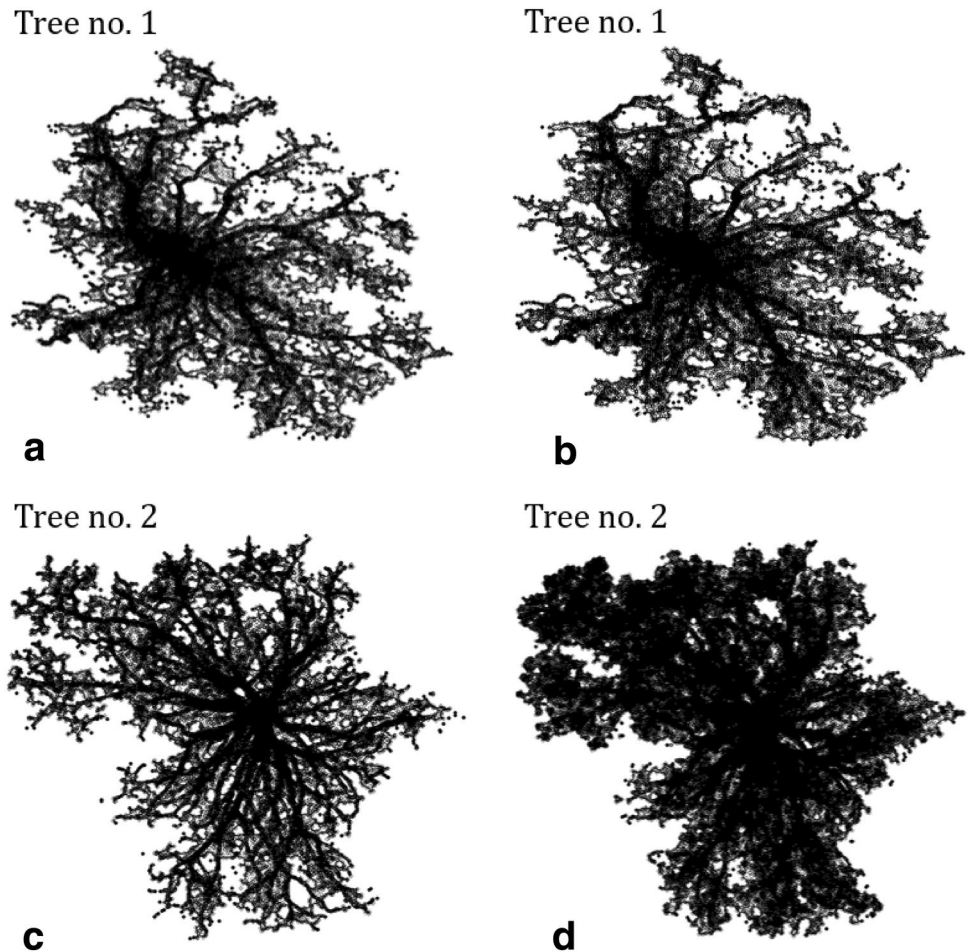
algorithm with noise (dbscan) function (Ester et al. 1996), obtained from the dbscan package of R (Hahsler and Piekenbrock 2019). We also used distance functions from the VoxR package for three-dimensional space (Lecigne et al. 2018). Afterwards, each tree was visually checked for completeness. If necessary, unrecognised tree parts were added manually, and artefacts that did not belong to the tree were removed using the software RiSCAN PRO version 2.10.1 (http://www.riegl.com/products/software-packages/riscan-pro/). Exact descriptions of the R packages used for the respective tasks are given in Appendix.

Foliation-describing parameter

Leaf area We used the difference between a tree's winter state and a tree's summer state after defoliation to calculate insect impact on foliation in insecticide-treated and control plots. Based on the TLS point clouds, total leaf area was calculated using the "alphahull" R package (Rodriguez-Casal and Pateiro-Lopez 2019). This package permitted the deter-

mination of the area and borderline of a sample of points in a plane, and it had also been successfully used in previous research to determine crown attributes (Jacobs et al. 2021; Rais et al. 2020). By varying the α-value, it was possible to adjust the tightness of the borderline around the point cloud. Very low α-values can even recognize areas without any points in the middle of a two-dimensional point set. When a uniform α-value of 0.1 was chosen, the polygon fitted tightly to the points (Fig. 6., Appendix). Subtracting each of the two subsequent areas from winter and summer, we obtained the periodic change of leaf area ($pc_{leaf\ area}$ in m²). It was essential to choose the same alpha values for the scans in leaf-off and leaf-on conditions to ensure the comparability of the measurements (*ceteris paribus* conditions). Repeated scanning campaigns of the same plots in 2019 made it possible to calculate the $pc_{leaf\ area}$ at the individual tree level. Via the difference between the horizontal projection area of the respective summer scanning campaign t_2 or t_3 and t_1 (Fig. 2), the $pc_{leaf\ area}$ of the individual tree could thus be calculated objectively in m² (Eqs. 1 and 2).

$$pc_{leaf\,area}, t_2 = \text{horizontal projection area}_{\alpha=0.1,\,t2} - \text{horizontal projection area}_{\alpha=0.1,\,t1} \qquad (1)$$

$$pc_{leaf\,area}, t_3 = \text{horizontal projection area}_{\alpha=0.1,\,t3} - \text{horizontal projection area}_{\alpha=0.1,\,t1} \qquad (2)$$

The leaf area$_i$ as the arithmetic mean of the periodic change for the individual tree is determined by Eq. 3:

$$\text{leaf area}_i = \left(pc_{leaf\,area}, t_2 + pc_{leaf\,area}, t_3\right)/2. \qquad (3)$$

Crown perforation In addition to the leaf area, we also calculated crown perforation from the data. The polygon can be used not only to derive an area but also to determine its length. To eliminate the size effect, the polygon length ($\alpha=0.1$) was divided by the crown projection area (*cpa*) area with $\alpha=1$ (Fig. 6). This result was finally divided by the polygon length of the *cpa* with $\alpha=1$ and multiplied by 100 (Eq. 4) to obtain the crown perforation as a percentage. The perforation of the crown is primarily determined by the length of the polygon ($\alpha=0.1$). The higher the polygon length (always in relation to crown size), the higher the perforation because more holes within the crown can then be found. The crowns are less compact in profile.

$$\text{Crown perforation}_{t2} = \frac{\left(\frac{Pl_{0.1}}{Pa_1}\right)}{Pl_1} * 100, \qquad (4)$$
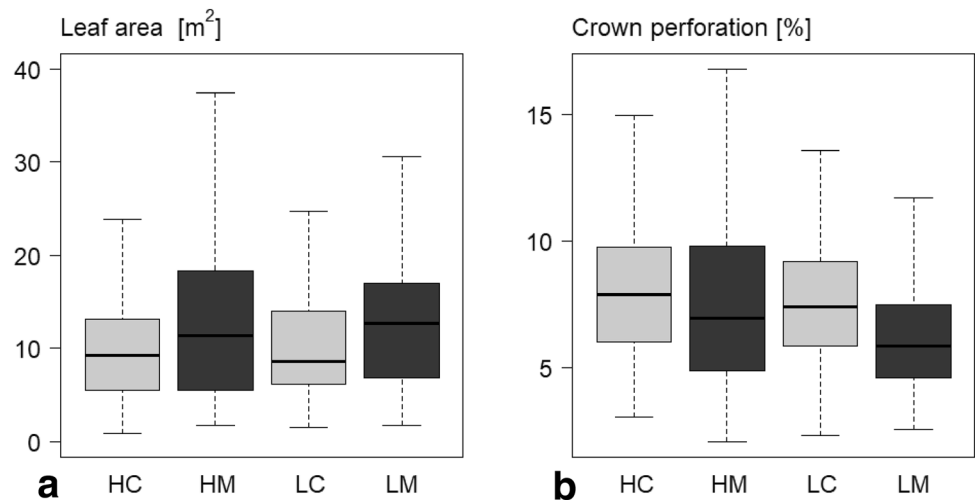
Statistics

Estimating leaf area, basal area increments, and crown perforation

We used the linear mixed-effects models to estimate the parameters for equations predicting leaf area, crown perforation, and basal area that form the basis for subsequent tests for the effect of gypsy moths on defoliation and tree growth (**Q1** and **Q3**). To analyse whether the leaf area and crown perforation calculated using TLS differ between trees attacked by gypsy moths and trees without damage (**Q1**), we created Eqs. 5 and 7, which used the foliation values of all 352 oak trees scanned at t_2 and t_3. Those 352 trees served as the basis for Eqs. 6 and 8 to predict (*pred()*) leaf area and crown perforation for all 880 central oak trees as linear predictors to analyse the relationship between leaf area/crown perforation and basal area increment modified by the gypsy moth (**Q3**). The basal area increment was calculated via the long-term girth tapes measured in the interval after defoliation (June 2019) until the end of the growing season 2019.

$$\ln(\text{leaf area}_{ijk}) = a_0 + a_1 * \ln(\text{basal area}) + a_2 * \text{defoliation risk} + a_3 * \text{treatment} + b_k + \varepsilon_{ijk} \qquad (5)$$

$$\ln(\text{basal area increment}_{ijk}) = a_0 + a_1 * \ln(\text{basal area}) + a_2 * \text{pred(leaf area)} + b_k + \varepsilon_{ijk} \qquad (6)$$

$$\ln(\text{crown perforatrion}_{ijk}) = a_0 + a_1 * \ln(\text{basal area}) + a_2 * \text{defoliation risk} + a_3 * \text{treatment} + b_k + \varepsilon_{ijk} \qquad (7)$$

$$\ln(\text{basal area increment}_{ijk}) = a_0 + a_1 * \ln(\text{basal area}) + a_2 * \text{pred(crown perforation)} + b_k + \varepsilon_{ijk} \qquad (8)$$

$t2$ = scanning campaign at high peak gypsy moth,

$Pl_{0.1}$ = Polygon length of the crown projection calculated with alpha = 0.1,

Pa_1 = Polygon area of the crown projection calculated with alpha = 1,

Pl_1 = Polygon length of the crown projection calculated with alpha = 1.

Throughout each model, the variable *i* indexes the tree, the variable *j* the plot, and the variable *k* the block. The variable a_o represents the model's intercept, the variables a_1 and a_2 represent the slope coefficients, while the variable b_k represents the random effect related to the blocks. All random effects were assumed to be normally distributed, with an expected mean of zero. The uncorrelated remaining errors are ε_{ijk}.

Fig. 3 Descriptive statistics boxplot of **a** leaf area $((t_2 + t_3)/2)$ in m^2 and **b** crown perforation (t_2) as a percentage per tree, depending on treatment and defoliation risk, measured using raw data after defoliation until the end of the growing season. The experiment comprised two defoliation risk levels, high (H) or low (L), and two treatment types, sprayed with Mimic (M) to protect the trees against defoliation or unsprayed control (C). The factorial design comprised the four combination types (HC, HM, LC and LM)

Descriptive statistics

We used boxplots to illustrate the distribution of the leaf area and crown perforation depending on treatment and defoliation risk to see the difference between trees attacked by gypsy moths and trees without damage (Q1). We performed correlation analyses to determine whether leaf area and crown perforation are related to stem increment within the same year (Q2). We decided to focus on the strength of the relationship between TLS foliation measurements and inter-annual stem growth because no accurate reference for the leaf area status was available. With Eqs. 9 and 10, we compared linear models of tree growth, expressed as inter-annual increments in the trees' basal area, which includes the time from defoliation until the end of the growing season.

$$\text{basal area increment}_i = a_0 + a_1 * \text{leaf area} + \varepsilon_i \quad (9)$$

$$\text{basal area increment}_i = a_0 + a_1 * \text{crown perforation} + \varepsilon_i \quad (10)$$

Results

Descriptive statistics

For a first graphical overview, the leaf area and crown perforation distribution over the four defoliation risk and treatment groups are displayed as boxplots in Fig. 3. The distribution of the leaf area and the crown perforation differed between the four combination types visually (HC, HM, LC, and LM). The plots sprayed with Mimic had higher median leaf area values and lower median crown perforation values than the control plots (Fig. 3a, b).

Table 3 Statistics from linear mixed-effects models for Q1 and Q3

| Function	(5)	(6)	(7)	(8)
Response variable	Ln (leaf area)	Ln (basal area increment)	Ln (crown perforation)	Ln (basal area increment)
Intercept	− 2.70***	− 2.91**	− 4.45***	+1.71
Ln (basal area)	+0.67***	+0.48**	− 0.33***	+0.20
Defoliation risk (low)	+0.02		− 0.11*	
Treatment (Mimic)	+0.2***		− 0.14**	
Pred (leaf area)		+0.07*		
Pred (crown perforation)				− 0.26***
R^2 (adjusted)	0.33	0.19	0.23	0.21

Ln () is the logarithmic transformation, and *pred* means predicted. The category of defoliation risk is divided into high vs. low and treatment is in control vs. Mimic; R^2 (adjusted) is the coefficient of multiple determination; Estimates and significance values are given, while all significance values are in bold type

*$p < 0.05$
**$p < 0.01$
***$p < 0.001$

Fig. 4 Comparison of basal area increment in cm² year⁻¹ measured by long-term girth tapes between June 2019 (after defoliation) and the end of the growing season 2019 with **a** leaf area in m² measured after defoliation, and **b** crown perforation in %. Every dot is a single tree, and every line represents the regression line of Eqs. 9 and 10
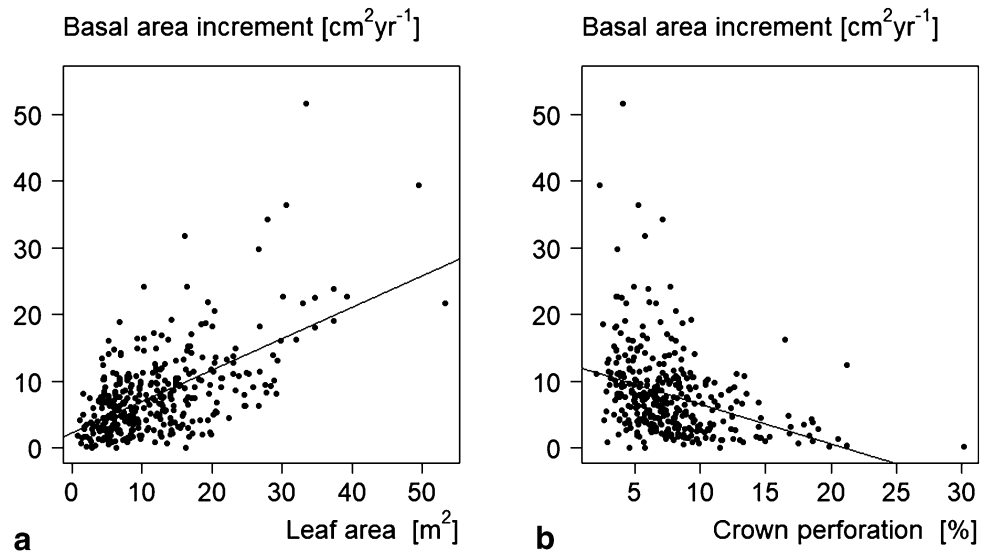
(Q1) Defoliation detection by TLS parameters

The results of the linear mixed-effects models are shown in Table 3. Regarding the leaf area, the estimation of the insecticide treatment parameter was significant, while the estimation of the defoliation risk parameter was not significant. For the crown perforation, the estimation of the treatment parameter and the defoliation risk parameter were significant. It can be seen that despite random effects on a block level, the estimation of the insect defoliation parameters affected leaf area and crown perforation (Fig. 3a, b, Table 3, Functions 5 and 7). Via TLS, we observed differences in leaf area and

crown perforation distribution on sprayed and control trees (Fig. 3a). The TLS-determined leaf area of trees on plots with no treatment was significantly lower than the tree's leaf area in the other treatment alternative (Table 3, Function 5). The estimated value of $+0.2$ for treated trees, shown in Table 3, Function 5, demonstrated this. Crown perforation differed significantly between control and treatment plots, as well as between high and low defoliation risk plots, and was higher in control plots and plots with a high defoliation risk (Table 3, Function 7). In Table 3, Function 7, the estimated values of -0.11 for treated trees and -0.14 for trees with a low defoliation risk also demonstrated this.
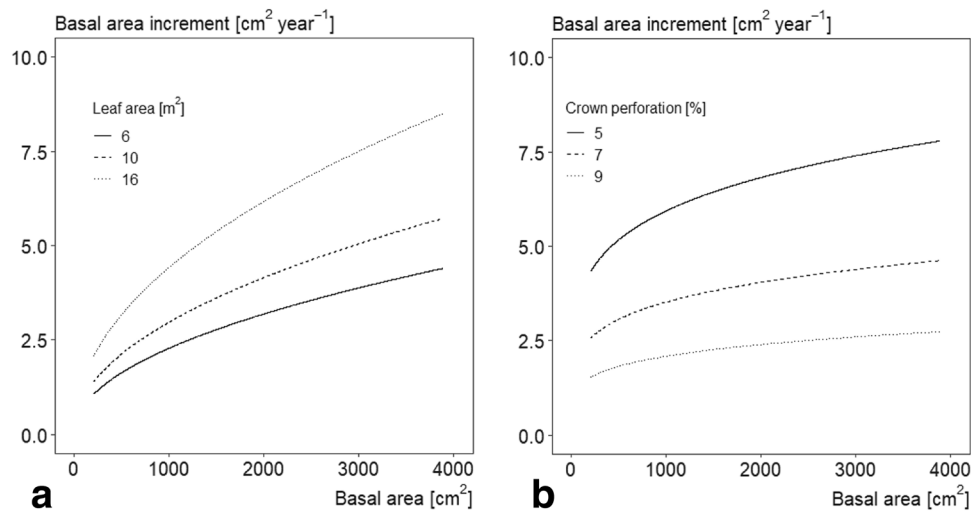

Fig. 5 Three curves for **a**) leaf area (m²) from Eq. 6 and **b** crown perforation (%) from Eq. 8 each depend on basal area increment in cm² year⁻¹ and basal area in cm². To create the three curves of **a**, the leaf area parameter from Eq. 6 was set to 6, the first quartile (=solid curve), then was set to 10, the median value (=dashed curve), and then was set to 16, the third quartile (=dotted curve) of all leaf area values. For the three curves of **b**, the crown perforation parameter from Eq. 8 was set to 5, the first quartile (=solid curve), then was set to 7, the median value (=dashed curve), and then was set to 9, the third quartile (=dotted curve) of all crown perforation values

(Q2) Correlation of basal area increment and foliation parameters

To answer the question, we decided to focus on the strength of the relationship between TLS foliation measurements and inter-annual stem growth, because no accurate reference for the leaf area status was available. At tree level, leaf area after defoliation was positively related to basal area increment (Fig. 4a, cor = + 0.6, $R^2 = 0.35$, $p < 0.001$), and the crown perforation negatively with basal area increment (Fig. 4b, cor = − 0.35, $R^2 = 0.12$, $p < 0.001$).

(Q3) Influence of defoliation on basal area increment

Oaks with a lower leaf area and higher crown perforation showed significant losses in the estimation of the basal area increment parameter compared to non-defoliated trees (Fig. 5a, b, Table 3, Functions 6 and 8). The growth losses depended in an almost linear way on crown perforation for trees at the lower end of the diameter range. However, non-linear effects occurred for trees at the upper end of the diameter range (Fig. 5a). Therefore, higher increment losses due to defoliation are expected for trees with a higher basal area (Fig. 5a). As for leaf area, higher increment losses due to higher crown perforation are expected for trees with a higher basal area (Fig. 5b). The curves of leaf area and crown perforation, from Functions 6 and 8, differ in intercept and slope. The slope of the leaf area curves is higher, while the curves of the crown perforation are separated from each other by a greater distance. Overall, they cover the same stem growth range. To create the curves, the first quartile, median, and third quartile values of all leaf area and crown perforation values were used to set them as leaf area and crown perforation parameters in Functions 6 and 8, respectively (Fig. 5).

Discussion

Defoliation detection by TLS

The high-resolution temporal monitoring of three-dimensional structures via repeated TLS scanning can deliver unique time-varying four-dimensional data of canopy structural dynamics (Calders et al. 2020). We used a TLS approach to detect defoliation and introduced the novel parameters of leaf area and crown perforation that can be used for further studies. Therefore, the structural tree crown variations could be directly visualised and linked to tree growth over the year. Using our approach in an experimental setting with plots differing in outbreak condition and pest control measures, our linear mixed-effects models (Table 3, Functions 5 and 7) show that leaf area was significantly higher in plots that were sprayed with Mimic, which protected the trees against defoliation by gypsy moth (Table 3, Function 5), while crown perforation was significantly lower

on these plots (Table 3, Function 7), resulting in fewer perforated and more compact crowns in leaf-on (t_2) condition. Previous studies into foliation detection via TLS have so far largely focused on the development of a methodology (Calders et al. 2020), with the aim of validating the approaches introduced, but these have not been used so far to identify stress-induced defoliation. On the other hand, some studies were able to show that TLS can detect defoliation at both the tree and stand level (Huo et al. 2019; Kaasalainen et al. 2010).

The evaluation of new automated approaches with an appropriate reference for validation is important in all cases. It would be ideal to measure each individual leaf of the crown, which is not possible due to time requirements and the difficulty of accessibility. Most of the studies used visual defoliation assessment as a reference for the validation of their estimated parameters (Huo et al. 2019; Kaasalainen et al. 2010). Even thorough training may not remove observer bias if multiple operators perform the assessment, and thus visual assessment is not a suitable reference. Any other ground-based measurement method is also not the ideal reference since the resulting foliation is only estimated. In contrast to the common TLS leaf-wood separation approaches and defoliation studies, we evaluated our calculated foliation parameters based on inter-annual stem growth, since stem growth and foliation are correlated (Rolland et al. 2001). In addition, stem growth is easy and accurate to measure in the field on the same tree that we used to calculate the foliation. The results of Ferretti et al. (2021) suggest that even slight and moderate variations in defoliation may have a significant impact on tree and forest growth. They found out that growth was inversely related to defoliation. Even lightly defoliated trees showed a significant reduction in growth (Ferretti et al. 2021). Both of our foliation-describing parameters correlated with the basal area increment, which was calculated within the same year directly after defoliation had taken place. As expected, leaf area was significantly and positively (Fig. 4a, cor = + 0.6, $R^2 = 0.35$, $p < 0.001$), and the crown perforation significantly and negatively (Fig. 4b, cor = − 0.35, $R^2 = 0.12$, $p < 0.001$) related to basal area increment. The reason for the lower correlation is probably that the crown perforation calculation was based on only one scanning campaign, whereas the leaf area determination method needed at least two and thus contained more information.

We cannot compare our results in terms of validation with other studies, as they mostly do visual assessments and do not consider stem growth as a reference. Regarding our results, the leaf area was the more suitable parameter for determining the foliation. The correlation of leaf area and basal area increment showed better results compared to crown perforation and basal area increment (Fig. 4a, b). Still, the crown perforation parameter was able to describe defoliation (Table 3, Function 7). Nevertheless, crown perforation seems to have a greater effect on stem growth, as shown by the significance and R^2 of Function 8 (Table 3). In addition, Function 7 (Table 3) shows

that crown perforation, in contrast to the leaf area, is significantly lower on plots where a low defoliation risk with a low density of gypsy moth eggs was found. Thus, the assessment of the defoliation risk based on egg-mass density, before the outbreak occurred was relatively accurate. The way the crown perforation describes the structure of the crown might give some clues about the current and past tree health. Perhaps the crown perforation not only offers the possibility to estimate foliation but also assess the tree's vitality due to the additional information on the crown's structural properties.

Defoliation and tree growth loss

Oaks with a decreasing leaf area and an increasing crown perforation revealed significant losses in basal area stem increment (Fig. 5a, b, Table 3, Functions 6 and 8). Our results are in line with the findings of Waring (1987), Dobbertin (2005) and Ferretti et al. (2021) who stated that insect defoliation affects the photosynthetic processes and reduces stem growth. Furthermore, due to the varying distances between the curves, we found that the growth losses, with decreasing leaf area and increasing crown perforation, were smaller at the lower end of the diameter range compared to the upper end of the diameter range (Fig. 5a, Table 3, Function 6). Hence, higher increment losses due to defoliation are expected for thicker trees that have a higher basal area (Fig. 5b, Table 3, Function 8).Usually, defoliation by insects initially becomes visible while stem growth reactions occur with a delay (Dobbertin 2005). The growth losses identified in this study were observed immediately after defoliation towards the end of the growing season. The plots integrated in this study did not suffer substantial defoliation in the previous years. Perhaps there are some long-term effects and the growth losses became even higher in the year after defoliation occurred.

Suitability of TLS and foliation-describing parameters

However, after critically reflecting, it becomes clear that working with TLS nevertheless has disadvantages. It can only be used in calm conditions without rain and fog, which reduces its temporal flexibility. This is especially true when capturing the exact time of peak defoliation is crucial. There is also a very large amount of data that needs to be processed. Still, we developed new rational measurement methods to determine the foliation of a tree with a fast and easy-to-understand procedure. However, there are a few limitations to our methods. Calculating the leaf area parameter is time consuming because at least two scanning campaigns are required, one in a leaf-off condition and one in a leaf-on condition. Nevertheless, the temporal monitoring of three-dimensional structures via repeated TLS scanning showed the potential to deliver time-varying defoliation data. The calculated crown perforation, which only requires one scanning

campaign, is not as strongly correlated with basal area increment as the calculated leaf area. Furthermore, the leaf area parameter is only applicable to deciduous trees because one scanning campaign without leaves is necessary. This is clearly not possible with evergreen trees. The parameter crown perforation is not limited by the need for only one scanning campaign, but the input has less information and hence is not as accurate in relation to the correlation results with basal area increment (Fig. 4).

The branch growth between scanning campaigns one and two could result in overestimating leaf area. However, this only affects the leaf area parameter since, as mentioned above, at least two scanning campaigns are needed as input, in contrast to the parameter crown perforation, which needs only one measurement.

Another point of criticism is that the two-dimensional analysis based on viewing from above certainly does not consider every single leaf within the crown (Fig. 2). Moreover, some studies state that TLS underestimates the heights of big trees, which may be due to the occlusion of the crown and stem parts (Wang et al. 2019). The occlusion problem can be largely resolved by choosing sufficient different scan positions (Wilkes et al. 2017). However, this problem shows that it is even more difficult to scan every single leaf of a tree crown that is shaded or covered by other trees in a dense stand. Hence, a robust and simple method is required that works even if not all the leaves in the crown are scanned. The situation is comparable to the recording of the LAI. It is always estimated but practically never measured. We developed two foliation describing parameters and successfully tested them in a large-scale field experiment in gypsy moth-infested oak-mixed forests in Germany, evaluating the results based on stem growth to demonstrate their performance. The next steps towards scaling up would be to test other age stages, size dimensions, other species, other pests, or stress factors, and to find a solution to calculate leaf area for evergreen trees.

Summary-applications, recommendations, and implications

Regarding our research questions, the leaf area and crown perforation calculated using TLS differed between trees attacked by gypsy moths and trees without damage. Within the same year, leaf area and crown perforation are related to stem increment. The relationship between leaf area/crown perforation and basal area increment was modified by the gypsy moth, causing foliation and stem growth loss.

Precise foliation surveys have high potential for better scientific understanding and modelling. For example, the leaf area index (LAI) is an important factor for estimating the primary productivity of a forest stand and thus important for forecasting the productivity of terrestrial ecosystems (Sato et al. 2007). Furthermore, other modelling approaches show that LAI may increase in mixed (Forrester et al. 2019) and fertilised forest

stands (Smethurst et al. 2003). The determination of defoliation is important to predict damage via pest-growth-models (Dietze and Matthes 2014), while leaf area is an important component for determining light absorption, whose accurate prediction is critical for many process-based forest growth models (Forrester et al. 2014). According to Dobbertin and Brang (2001), including defoliation can considerably improve the prediction accuracy of models that predict tree mortality based solely on competition indicators and tree size.

Conclusions

Our results show that TLS can offer new opportunities for calculating foliation at the individual tree level. On the one hand, this study could be a step forward towards a more objective and personal independent foliation estimation, which is easier to understand in comparison to other TLS approaches. On the other hand, our results demonstrated that iterative TLS surveys might enhance the information gathered during measuring campaigns on common long-term experimental plots by obtaining a more thorough picture of growth patterns resulting from insect defoliation. The new approach detected the defoliation via leaf area caused by the gypsy moths and revealed subsequent growth losses during the same year. The crown perforation foliation parameter can describe the defoliation or even the vitality status of a single tree based on only one scanning campaign, whereas our leaf area determination method needs at least two. Since it is impossible to scan every single entire leaf of a crown, robust and simple methods are required that work even if not all the leaves in the crown are scanned. Still, robust and ready-to-use software for TLS data post-processing is not available, so the ability to program is necessary.

Author contribution statement

MJ: conceptualization, data collection, data curation, TLS processing, formal analysis, investigation, methodology, resources, software, validation, visualization, writing-original draft, writing-review and editing. TH: conceptualization, data collection, data curation, methodology, visualization, writing—review and editing. BMLL: conceptualization, methodology, writing—review and editing. SK: conceptualization. HL: conceptualization, writing—review and editing. JM: supervision, conceptualization, resources, writing—review and editing. WWW: supervision, conceptualization, resources, writing—review and editing. HP: supervision, conceptualization, methodology, resources, writing—original draft, writing—review and editing.

Appendix

See Table 4.

Table 4 Stand characteristics of the 44 plots in Franconia-Bavaria, Germany

Plot	n (ha^{-1})	dq (cm)	hq (m)	BA (m^2 ha^{-1})	Standing stock (m^3 ha^{-1})
AHC	713	20.2	15.9	27.5	218.3
AHM	339	27.7	19.6	23.5	230.2
ALC	603	20.7	17.2	27.8	239.1
ALM	476	23.5	17.6	30.1	265.0
BHC	314	27.5	18.8	22.5	211.1
BHM	459	26.3	20.6	30.5	313.5
BLC	406	25.1	19.5	23.8	232.4
BLM	622	23.2	20.2	30.3	305.2
DHC	615	23.8	18.2	40.1	364.6
DHM	357	26.5	18.6	27.7	258.0
DLC	753	21.6	17.2	38.9	334.1
DLM	744	19.9	15.7	35.3	276.4
FHC	243	31.1	21.2	22.7	240.3
FHM	467	25.1	19.0	36.4	345.8
FLC	200	40.9	26.8	27.8	373.3
FLM	244	36.4	24.4	29.0	353.0
GHC	438	23.8	16.0	28.8	230.5
GHM	261	33.5	21.8	27.7	301.0
GLC	513	22.0	17.2	30.1	258.3
GLM	632	19.4	16.1	29.0	233.3
HHC	437	29.1	22.0	33.6	369.5
HHM	528	24.9	19.1	31.5	300.7
HLC	503	26.5	21.0	29.0	305.2
HLM	640	24.7	20.2	34.3	346.3
JHC	552	25.5	19.8	35.2	348.4
JHM	718	20.8	19.0	29.7	281.3
JLC	382	26.7	22.1	25.8	284.8
JLM	294	31.7	22.3	31.9	356.5
MHC	512	27.2	21.2	41.7	443.0
MHM	323	30.2	22.1	28.7	317.7
MLC	503	27.7	20.7	39.1	404.8
MLM	369	30.2	19.5	35.1	342.2
NHC	475	25.0	17.8	28.6	254.4
NHM	359	25.6	18.2	25.1	228.1
NLC	433	25.1	18.1	30.1	272.5
NLM	293	29.1	19.9	24.9	247.1
OHC	394	27.0	18.5	29.0	267.1
OHM	672	23.2	17.1	36.1	309.2
OLC	214	33.9	23.2	23.8	275.7
OLM	190	33.3	22.4	20.5	230.5
SHC	296	31.7	21.5	32.6	349.7
SHM	325	28.6	20.8	30.1	313.0
SLC	312	30.1	23.3	26.9	313.6
SLM	298	29.2	23.2	26.3	305.4

The parameters were calculated based on TLS point clouds using 5280 trees (six-tree subplots). The plots are characterised by block/defoliation risk/treatment

n number of trees, dq quadratic mean diameter, hq height corresponding to dq, BA basal area

Table 5 Overview of the RIEGL VZ-400i (RIEGL 2019), summarising the main characteristics

Laser measurement system (LMS) LMS		RIEGL VZ-400i
Range[a]	m	800
Effective measurement rate[b]	meas./sec	500,000
Accuracy[c,d]	mm	5
Precision[d,e]	mm	3
Vertical field of view		100
Pulse mode		Multiple target capability
Registration		Automatic
Laser beam divergence	mrad	0.35[f]

[a]Typical values for average conditions. Maximum range is specified for flat targets with size in excess of the laser beam diameter, perpendicular angle of incidence, and for atmospheric visibility of 23 km. In bright sunlight, the max. Range is shorter than under overcast sky

[b]Rounded values

[c]Accuracy is the degree of conformity of a measured quantity to its actual (true) value

[d]One sigma at 100 m range under RIEGL test conditions

[e]Precision, also called reproducibility or repeatability, is the degree to which further measurements show

[f]Measured at the 1/e2 points. 0.35 mrad corresponds to an increase of 35 mm of beam diameter per 100 m distance

Defoliation risk index (Leroy et al. 2021)

The defoliation risk index (DRI) was calculated as:

$$DRI = \frac{MEM}{CEM_c}$$

MEM is the average number of egg masses per stem, while CEMc is the corrected critical egg-mass density for the focal survey transect. Stands with a defoliation risk index > 1 had a high risk of defoliation, while a defoliation risk index < 0.5 was considered low risk. The results were extrapolated to the surrounding areas to identify candidate sites for the experiment, i.e., stands with high DRI (> 1) and low DRI (0.5) that were close enough to one another to be grouped into experimental blocks (maximum inter-plot distance within-block of 10 km).

TLS procedure of data acquisition and parameter extraction

Scanner configuration and settings

The RIEGL VZ-400i (RIEGL 2019) laser measurement system was used. An overview of the main scanner characteristics is provided in Table 5.

We used a laser pulse repetition rate of 1200 kHz. One horizontal 360° scan was performed for each scan position with
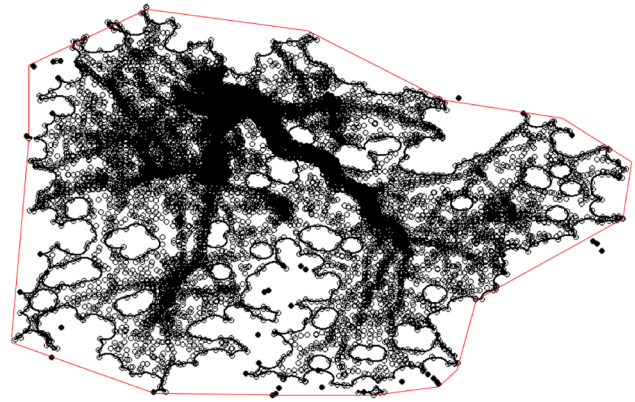

Fig. 6 A top view of an oak tree. By way of illustration of the different methods for calculating the leaf area and crown perforation within the R package "alphahull". Choosing an α-value of 1 (red polygon), a projection area similar to the traditional crown projection area was derived. Choosing an α-value of 0.1 (black polygon), the polygon framed the crown tightly

a 100° vertical field of view. In our practical experience, the horizontal angular resolution was set to 0.04°, which in our practical experience, achieves a reasonable trade-off between scan-time (45 s per scan) and the risk of disturbances due to tree movement through wind. Due to the angular measurement scheme of the scanner, which operates from the ground, the point density naturally decreases towards the top of the canopy. Furthermore, the laser beam is usually unable to penetrate tree compartments to perform measurements behind obstacles. These two effects result in rather sparse measurement densities in the upper crown and stem regions, especially if the crown parts near the scanner are dense (Hilker et al. 2010). Using the pulsed time-of-flight method for laser range measurements, the RIEGL LMS VZ-400i determines the range to all targets with which a single laser pulse interacts ("multi-target capability"). Depending on the measurement program used, the maximum number of targets that can be detected varies (typically 4–15). The RIEGL LMS VZ-400i can generate 4–15 points per laser beam.

Data post-processing

We did not focus on three-dimensional tree features. Instead, our crown target variables (leaf area and crown perforation) were two-dimensional to take into account that not every individual leaf within the crown can be scanned. This was done to exclude errors occurring in the three-dimensional analysis due to non-scanned areas of the upper crown region, respectively. Using the software RiSCAN PRO version 2.0.2 (http://www.riegl.com/products/software-packages/riscan-pro/), all scan positions per plot were co-registered. The new automatic registration of the LMS VZ-400i was used so that

artificial reference targets were no longer needed. Automatic registration and filtering were performed using the software RiSCAN PRO version 2.8.2.

Tree detection and isolation

To detect individual-tree positions, we used the density-based spatial clustering algorithm with noise (dbscan) function in the dbscan package of R (Hahsler and Piekenbrock 2017). The function relied on a density-based notion of clusters, which was designed to discover clusters of arbitrary shape (Ester et al. 1996). Only the x- and y-axes were used as input data, thereby pushing all points belonging to the z-axis to one height level. The consequence was a higher point density per tree stem. Now dbscan is automatically able to find each tree as a cluster. This meant that each recognized cluster (stem) now received a unique number and could be processed individually. Additionally, non-vertically grown trees were detected at the lower part of the stem. Ground points were recognized by dbscan as noise points because of their horizontal structure in contrast to the vertically grown stems. For each stem cluster, stem base points were determined. The median values of the x- and y-coordinates and the minimum value of the z-axis of the stems were calculated. The stem base points now serve to extract the original points of the entire tree. The isolation of each single tree from the TLS point cloud was performed using the dbscan algorithm within the R programming environment (R Core Team 2016). With the application of dbscan, the entire point cloud was classified into clusters. Now each cluster is individually queried, which stem base cluster is closest in distance and whether this distance is close enough to be classified as associated points. After this step, each tree was visually checked for completeness. If necessary, unrecognised tree parts were added manually, and artefacts that did not belong to the tree were removed using the software RiSCAN PRO (http://www.riegl.com/products/software-packages/riscan-pro/).

Tree parameter extraction

The total tree height is calculated by determining the z-axis minimum and maximum points of the isolated tree. The minimum value is subtracted from the maximum value, and the output is the height. Wang et al. (2019) reported that TLS underestimated the height of big trees, which may be due to occlusion of crown and stem parts. The occlusion problem might be mainly resolved by choosing a sufficient number of different scan positions. On the other hand, TLS height measurements on Norway spruce trees in forest stands that covered a broad density range were found to be more accurate than common height measurements with the Vertex, a hand-held device based on the trigonometrical principle (Jacobs et al. 2020). Regarding our study, the total tree heights were obtained from the pointclouds in a leaf-off condition in winter. The number of scan positions per plot varied from 80 to 110 depending on stand density. Therefore, the occlusion problem should be reduced to an absolute minimum. The procedure applied for diameter calculation was introduced in Jacobs et al. (2020).

Availability of data and materials All data and materials support the published claims and comply with field standards. The datasets generated during and/or analysed during the current study are available from the corresponding author on reasonable request.

Code availability Not applicable.

Declarations

Conflict of interest The authors declare that they have no known competing financial interests or personal relationships that could have appeared to influence the work reported in this paper.

Ethical approval Not applicable.

Consent to participate All authors obtained consent to participate.

Consent for publication All listed authors have approved the manuscript before submission.

References

Bayer D, Seifert S, Pretzsch H (2013) Structural crown properties of Norway spruce (*Picea abies* [L.] Karst.) and European beech (*Fagus sylvatica* [L.]) in mixed versus pure stands revealed by terrestrial laser scanning. Trees 27:1035–1047. https://doi.org/10.1007/s00468-013-0854-4

Blank R (1997) Ringporigkeit des Holzes und häufige Entlaubung durch Insekten als spezifische Risikofaktoren der Eichen. Forst Und Holz 52:235–242

Bradshaw CJA, Leroy B, Bellard C, Roiz D, Albert C, Fournier A, Barbet-Massin M, Salles J-M, Simard F, Courchamp F (2016) Massive yet grossly underestimated global costs of invasive insects. Nat Commun 7:12986. https://doi.org/10.1038/ncomms12986

Calders K, Adams J, Armston J, Bartholomeus H, Bauwens S, Bentley LP, Chave J, Danson FM, Demol M, Disney M, Gaulton R, Krishna Moorthy SM, Levick SR, Saarinen N, Schaaf C, Stovall A, Terryn L, Wilkes P, Verbeeck H (2020) Terrestrial laser scanning in forest ecology: expanding the horizon. Remote Sens Environ 251:112102. https://doi.org/10.1016/j.rse.2020.112102

Dietze MC, Matthes JH (2014) A general ecophysiological framework for modelling the impact of pests and pathogens on forest ecosystems. Ecol Lett 17:1418–1426. https://doi.org/10.1111/ele.12345

Dobbertin M (2005) Tree growth as indicator of tree vitality and of tree reaction to environmental stress: a review. Eur J Forest Res 124:319–333. https://doi.org/10.1007/s10342-005-0085-3

Dobbertin M, Brang P (2001) Crown defoliation improves tree mortality models. For Ecol Manag 141:271–284. https://doi.org/10.1016/S0378-1127(00)00335-2

Dobbertin M, Hug C, Waldner P (2009) Kronenverlichtung, Sterberaten und Waldwachstum in Langzeitstudien – Welche Indikatoren beschreiben den Waldzustand am besten? Forum für Wissen 7–20

Eckmüllner O, Sterba H (2000) Crown condition, needle mass, and sapwood area relationships of Norway spruce (*Picea abies*). Can J for Res 30:1646–1654

Elling W, Heber U, Polle A, Beese F (2007) Schädigung von Waldökosystemen: Auswirkungen anthropogener Umweltveränderungen und Schutzmaßnahmen. Elsevier, Spektrum Akad. Verlag

Elseberg J, Borrmann D, Nüchter A (2013) One billion points in the cloud – an octree for efficient processing of 3D laser scans. ISPRS J Photogramm Remote Sens 76:76–88. https://doi.org/10.1016/j.isprsjprs.2012.10.004

Ester M, Kriegel HP, Sander J, Xu X (1996) A density-based algorithm for discovering clusters in large spatial databases with noise. In kdd 96(34):226–231

Fajvan MA, Wood JM (1996) Stand structure and development after gypsy moth defoliation in the Appalachian Plateau. For Ecol Manag 89:79–88. https://doi.org/10.1016/S0378-1127(96)03865-0

Fajvan MA, Rentch J, Gottschalk K (2008) The effects of thinning and gypsy moth defoliation on wood volume growth in oaks. Trees 22:257–268. https://doi.org/10.1007/s00468-007-0183-6

Ferretti M, Bacaro G, Brunialti G, Calderisi M, Croisé L, Frati L, Nicolas M (2021) Tree canopy defoliation can reveal growth decline in mid-latitude temperate forests. Ecol Ind 127:107749. https://doi.org/10.1016/j.ecolind.2021.107749

Forrester DI, Guisasola R, Xea T (2014) Using a stand-level model to predict light absorption in stands with vertically and horizontally heterogeneous canopies. For Ecosyst 1:1–19

Forrester DI, Rodenfels P, Haase J, Härdtle W, Leppert KN, Niklaus PA, von Oheimb G, Scherer-Lorenzen M, Bauhus J (2019) Tree-species interactions increase light absorption and growth in Chinese subtropical mixed-species plantations. Oecologia 191:421–432. https://doi.org/10.1007/s00442-019-04495-w

Gieger T, Thomas FM (2002) Effects of defoliation and drought stress on biomass partitioning and water relations of *Quercus robur* and *Quercus petraea*. Basic Appl Ecol 3:171–181. https://doi.org/10.1078/1439-1791-00091

Gninenko YI, Orlinskii AD (2003) Outbreaks of *Lymantria dispar* in Russian forests during the 1990s. EPPO Bull 33:325–329

Hahsler M, Piekenbrock M (2019) dbscan: density based clustering of applications with noise (DBSCAN) and related algorithms. J Stat Soft. https://doi.org/10.18637/jss.v091.i01

Hilker T, van Leeuwen M, Coops NC, Wulder MA, Newnham GJ, Jupp DLB, Culvenor DS (2010) Comparing canopy metrics derived from terrestrial and airborne laser scanning in a Douglas-fir dominated forest stand. Trees 24:819–832. https://doi.org/10.1007/s00468-010-0452-7

Huo L, Zhang N, Zhang X, Wu Y (2019) Tree defoliation classification based on point distribution features derived from single-scan terrestrial laser scanning data. Ecol Indic 103:782–790

Innes JL (1993) Forest health: its assessment and status. CAB International

Jacobs M, Rais A, Pretzsch H (2020) Analysis of stand density effects on the stem form of Norway spruce trees and volume miscalculation by traditional form factor equations using terrestrial laser scanning (TLS). Can J for Res 50:51–64. https://doi.org/10.1139/cjfr-2019-0121

Jacobs M, Rais A, Pretzsch H (2021) How drought stress becomes visible upon detecting tree shape using terrestrial laser scanning (TLS). For Ecol Manag 489:118975. https://doi.org/10.1016/j.foreco.2021.118975

Kaasalainen S, Hyyppä J, Karjalainen M, Krooks A, Lyytikäinen-Saarenmaa P, Holopainen M, Jaakkola A (2010) Comparison of terrestrial laser scanner and synthetic aperture radar data in the study of forest defoliation. In: Wagner W, Székely B (eds) ISPRS TC VII Symposium – 100 Years ISPRS, Vienna, Austria, July 5–7, 2010, IAPRS, Vol. XXXVIII, Part 7A

Lecigne B, Delagrange S, Messier C (2018) Exploring trees in three dimensions: VoxR, a novel voxel-based R package dedicated to analysing the complex arrangement of tree crowns. Ann Bot 121(4):589–601. https://doi.org/10.1093/aob/mcx095

Leroy BML, Lemme H, Braumiller P, Hilmers T, Jacobs M, Hochrein S, Kienlein S, Müller J, Pretzsch H, Stimm K, Seibold S, Jaworek J, Hahn WA, Müller-Kroehling S, Weisser WW (2021) Relative impacts of gypsy moth outbreaks and insecticide treatments on forest resources and ecosystems: an experimental approach. Ecol Solut Evid. https://doi.org/10.1002/2688-8319.12045

Liebhold AM, Halverson J, Elmes G (1992) Quantitative analysis of the invasion of gypsy moth in North America. J Biogeogr 19:513–520

Logan JA, Régnière J, Powell JA (2003) Assessing the impacts of global warming on forest pest dynamics. Front Ecol Environ 1:130–137

McManus M, Csóka G (2007) History and impact of gypsy moth in North America and comparison to recent outbreaks in Europe. Acta Silv Lignaria Hung 3:47–64

Montgomery ME, Wallner WE (1988) Dynamics of forest insect populations. Plenum Press

Müller-Edwards C, Vries WD, Erisman JW (1997) Ten years of monitoring forest condition in Europe. Studies on temporal development, spatial distribution and impacts of natural and anthropogenic stress factors. UN/ECE

Naidoo R, Lechowicz MJ (2001) Effects of gypsy moth on radial growth of deciduous trees. For Sci 47:338–348

Nakajima H (2015) Defoliation by gypsy moths negatively affects the production of acorns by two Japanese oak species. Trees 29:1559–1566. https://doi.org/10.1007/s00468-015-1237-9

Orozumbekov AA, Liebhold AM, Ponomarev VI, Tobin PC (2009) Gypsy moth (*Lepidoptera*: *Lymantriidae*) in Central Asia. Am Entomol 55:258–265. https://doi.org/10.1093/ae/55.4.258

Pasquarella VJ, Elkinton JS, Bradley BA (2018) Extensive gypsy moth defoliation in Southern New England characterized using Landsat satellite observations. Biol Invasions 20:3047–3053. https://doi.org/10.1007/s10530-018-1778-0

Piper FI, Gundale MJ, Fajardo A (2015) Extreme defoliation reduces tree growth but not C and N storage in a winter-deciduous species. Ann Bot 115:1093–1103. https://doi.org/10.1093/aob/mcv038

R Core Team (2016) R: a language and environment for statistical computing. R Foundation for Statistical Computing, Vienna, Austria

Rais A, Pretzsch H, van de Kuilen J-WG (2020) European beech log and lumber grading in wet and dry conditions using longitudinal vibration. Holzforschung. https://doi.org/10.1515/hf-2019-0227

RIEGL (2019) Laser measurement system. (http://www.riegl.com,http://www.riegl.com/uploads/tx_pxpriegldownloads/RIEGL_VZ-400i_Datasheet_2020-10-06.pdf. Accessed 10 Nov2021

Rodriguez-Casal A, Pateiro-Lopez B (2019) alphahull: generalization of the convex hull of a sample of points in the plane. R package version 2.2. https://CRAN.R-project.org/package=alphahull

Rolland C, Baltensweiler W, Petitcolas V (2001) The potential for using Larix decidua ring widths in reconstructions of larch budmoth (*Zeiraphera diniana*) outbreak history: dendrochronological estimates compared with insect surveys. Trees 15:414–424. https://doi.org/10.1007/s004680100116

Roussel JR, de Boissieu F (2019) rlas: read and write "las" and "laz" binary file formats used for remote sensing data. R package version 1.3.4

Sato H, Itoh A, Kohyama T (2007) SEIB–DGVM: a new dynamic global vegetation model using a spatially explicit individual-based approach. Ecol Model 200:279–307. https://doi.org/10.1016/j.ecolmodel.2006.09.006

Seidel D, Schall P, Gille M, Ammer C (2015) Relationship between tree growth and physical dimensions of *Fagus sylvatica* crowns assessed from terrestrial laser scanning. iForest 8:735–742. https://doi.org/10.3832/ifor1566-008

Seidl R, Schelhaas M-J, Lexer MJ (2011) Unraveling the drivers of intensifying forest disturbance regimes in Europe. Glob Chang Biol 17:2842–2852. https://doi.org/10.1111/j.1365-2486.2011.02452.x

Smethurst P, Baillie C, Cherry M, Holz G (2003) Fertilizer effects on LAI and growth of four *Eucalyptus nitens* plantations. For Ecol Manag 176:531–542. https://doi.org/10.1016/S0378-1127(02)00226-8

Thomas FM, Blank R, Hartmann G (2002) Abiotic and biotic factors and their interactions as causes of oak decline in Central Europe. For Pathol 32:277–307. https://doi.org/10.1046/j.1439-0329.2002.00291.x

Villemant C, Ramzi H (1995) Predators of *Lymantria dispar* egg masses: spatio-temporal variation of their impact during the 1988–89 pest generation in the mamora cork oak forest (Morocco). Entomophaga 40:441–456

Wang Y, Pyörälä J, Liang X, Lehtomäki M, Kukko A, Yu X, Kaartinen H, Hyyppä J (2019) In situ biomass estimation at tree and plot levels: what did data record and what did algorithms derive from terrestrial and aerial point clouds in boreal forest. Remote Sens Environ 232:111309. https://doi.org/10.1016/j.rse.2019.111309

Waring RH (1987) Characteristics of trees predisposed to die. Bioscience 37:569–574

Watanabe Y, Ohno Y (2020) Severe insect defoliation at different timing affects cell wall formation of tracheids in secondary xylem of *Larix kaempferi*. Trees 34:931–941. https://doi.org/10.1007/s00468-020-01971-2

Wilkes P, Lau A, Disney M, Calders K, Burt A, Gonzalez de Tanago J, Bartholomeus H, Brede B, Herold M (2017) Data acquisition considerations for terrestrial laser scanning of forest plots. Remote Sens Environ 196:140–153. https://doi.org/10.1016/j.rse.2017.04.030

Wulff S (2002) The accuracy of forest damage assessments–experiences from Sweden. Environ Monit Assess 74:295–309